Viscoelastic Two-Dimensional Modeling of Cell Deformation Due to Shear Stress on Apical Focal Adhesion, with Experimental Design Considerations

by

Jeffrey J. Hsu

SUBMITTED TO THE DEPARTMENT OF MECHANICAL ENGINEERING IN PARTIAL FULFILLMENT OF THE REQUIREMENTS FOR THE DEGREE OF

BACHELOR OF SCIENCE IN MECHANICAL ENGINEERING
AT THE
MASSACHUSETTS INSTITUTE OF TECHNOLOGY

JUNE 2005

Signature of Author .....
Department of Mechanical Engineering
May 6, 2005

Certified by .....
Roger D. Kamm
Professor of Mechanical Engineering and Biological Engineering, MIT
Thesis Co-Supervisor

Certified by .....
Mohammad R. Kaazempur-Mofrad
Assistant Professor of Bioengineering, University of California, Berkeley
Thesis Co-Supervisor

Accepted by .....
Ernest G. Cravalho
Professor of Mechanical Engineering, MIT
Chairman, Undergraduate Thesis Committee

This page intentionally left blank.

PAGES (S) MISSING FROM ORIGINAL

PAGES 3 AND 4 ARE MISSING

Acknowledgements

For their support throughout the work and writing of this thesis, I would like to thank my thesis supervisors, Dr. Kaazempur Mofrad and Prof. Kamm. Their guidance over the past several months has been invaluable, and I thank them for exposing me to the groundbreaking work being conducted in the exciting field of mechanotransduction.

Also, I would like to thank the other members of the Kamm Lab who have acquainted me with the laboratory procedures and have provided me with numerous answers to my numerous questions. In particular, the assistance of Nur Aida Abdul Rahim, Peter Mack, Vernella Vickerman, Helene Karcher, Alisha Siemenski, and Belinda Yap has been much appreciated.

Lastly, I want to thank members of other labs who have helped me with the execution of this thesis: Nate Tedford (Griffith Lab) for his assistance with the FEMLAB software, and Judith Su (So Lab) for providing me with the beads used in my experiments.

This page intentionally left blank.

List of Contents

List of Figures

List of Tables

This page intentionally left blank.

1.0 INTRODUCTION

Cells are exposed to a wide variety of forces within the human body, and the mechanisms by which cells respond to these forces are largely unknown. From altering gene transcription in the cell nucleus to conformational changes in membrane channel proteins that lead to increased or decreased ion permeability, external stresses imposed on the cell can significantly affect cellular actions through a process known as "mechanotransduction." While such cellular actions include fundamental processes such as cell motility and protein production, the cellular response to external forces can also be pathogenic. For instance, plaque formation within the arteries often occurs at points where the arteries branch or bend sharply, or rather, where cells are subjected to low or reversing fluid shear stresses [1, 2]. Atherosclerosis, one of the leading causes of cardiovascular disease, is the result, and it is it has been well established that shear stress is a primary factor influencing a number of endothelial signaling pathways that contribute to the onset of disease. In addition, asthma research, as one other particularly salient example, could benefit from such a study. The epithelial cells lining the airways are subjected to stresses as the pulmonary airways constrict as a result of smooth muscle activation, and airway wall remodeling is a potential mechanotransduced result [3, 4]. Further knowledge of the mechanisms by which cells respond to such forces could enhance our understanding of these specific diseases, as well as numerous others.

One approach to understanding these mechanisms is to model a single cell's responses to mechanical stresses. While the mechanical behavior of the cell are still being studied, experimentally-found mechanical properties of the cell have been elucidated, making it possible to create a three-dimensional finite element model (FEM)

of a human cell. Examining the stress and strain responses of the cell to various external stresses will increase our understanding of the mechanics of the cell as well as the local forces involved with mechanotransduction.

Currently, three-dimensional models of the cell have been constructed using various finite element modeling programs such as ADINA (Watertown, MA) and ANSYS (Palo Alto, CA) [5, 6]. A program called FEMLAB (Comsol, Burlington, MA) has also garnered interest in the biomechanical modeling arena. Operating within the MATLAB (Mathworks, Natick, MA) framework, FEMLAB allows for a wide variety of finite element modeling capabilities that other programs fail to offer. One particularly important feature is the modeling of mass transport within the model. As the cellular membrane and intracellular environment consist of a dynamic mass, the modeling of the mass transport that occurs when the cell is subjected to external stresses is essential to understanding the cell's mechanics. Also, FEMLAB offers the modeling of porous media, a feature that is particularly useful in modeling the complex network of microfilaments of the intracellular environment or porous extracellular matrix.

1.1 Objective

The objective of this thesis is two-fold. First, the efficacy of the FEMLAB software in producing a robust FEM of a cell is examined. A two-dimensional continuum model is presented here, preparing the foundation for further development into a three-dimensional model. Secondly, the experimental design of an assay that analyzes the effects of a combination of fluid shear stress at the apical surface of an endothelial cell and the torsional stresses applied by an attached, rotating bead is discussed. The

designed assay looks specifically at the activity of focal adhesion sites in endothelial cells in response to the forces mentioned. While similar rotational and translational forces have previously been applied to integrin-bound beads to study the resulting cellular response, the combined study of a bead's rotational motion and fluid shear stress has not yet been conducted; a deeper insight into this combined effect is a primary goal of this thesis.

2.0 BACKGROUND

Although much remains unknown about the mechanisms of mechanotransduction, recent work has shed light on the different components of the possible pathways involved. In addition, FEMs developed in conjunction with experimental results have allowed for an understanding of how applied forces are transmitted throughout the cell. Determining the force distribution throughout the cell and comparing it to the actual cellular response can provide for key insights into mechanotransduction events.

2.1 Focal Adhesion Sites

Several theories have arisen in the attempt to delineate the physical basis of mechanotransduction. Previous hypotheses have proposed that stresses elicit cellular responses by means such as altering the fluidity of the membrane, thereby allowing membrane-bound protein receptors to aggregate and initiate signal transduction [7]. Others have identified stress-induced conformational changes in ion channel proteins as a probable source of the mechanotransduced effects [8]. More recent work has focused on the activity and mechanics of focal adhesion sites in the force transmission pathway [9-

11], as their rapid response to mechanical stimulation and their localization to sites of stimulation make them the likely initiators of cellular mechanosensing.

A class of transmembrane proteins known as integrins is found in the cellular membrane as α/β heterodimers, with sites exposed to both the extracellular and intracellular environments. In cell adhesion, integrin proteins' extracellular domains bind to ligands in the extracellular matrix (ECM). Upon binding, proteins are recruited to the cytoplasmic domains of integrins, forming chains that ultimately link the ECM with the cellular actin cytoskeleton. These clusters constitute focal adhesion sites and consist of proteins such as focal adhesion kinase (FAK), Src, paxillin, tensin, vinculin, and talin, to name a few. A schematic of one group of focal adhesion proteins is shown in Figure 2.1.

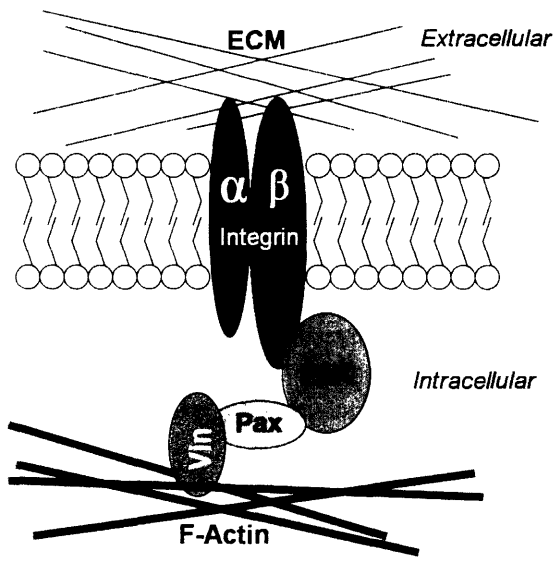

Figure 2.1: Schematic of a sample of proteins involved in focal adhesion sites. The diagram presents some of the many proteins involved in the integrin / focal adhesion interaction with the extracellular matrix (ECM). The α/β-integrin heterodimer incorporated into the cellular membrane binds to the ECM. In response, proteins are recruited to the integrin proteins to form a focal adhesion. Here, focal adhesion kinase (FAK) binds to the β-integrin of the heterodimer, resulting in a binding cascade that includes the proteins paxillin (Pax) and vinculin (Vin), the latter of which is bound to the actin cytoskeleton. The focal adhesion site thereby provides a connection between the ECM and the internal structural architecture.

In addition, focal adhesion sites have been identified as sources of signaling; their activation triggers signaling pathways involving Rho-family GTPases, which induce focal adhesion formation and strengthening via protein recruitment [12-14]. Experiments using the fluorescent tagging of proteins or reporters (such as paxillin with GFP, Src reporter with CFP and YFP) to visualize focal adhesion activation in cells have shown that the focal adhesion response to applied forces is quick and global, but varies with the location and magnitude of force [9, 11]. Translocation of the complexes can be seen throughout the cell minutes after localized stresses are imposed upon a single focal adhesion site on the apical surface. Furthermore, forces on integrins have been shown to induce changes in gene expression; Chen et al discovered an increased expression of the gene *endothelin*-1 after twisting integrin proteins of endothelial cells [15]. Such results support the notion that focal adhesion sites play a major role in the cell's mechanosensing functions.

Several mechanical tests have been performed on focal adhesions, analyzing their mechanical properties and force transmission abilities. To isolate applied forces to a single focal adhesion site, most of these tests have utilized fibronectin-coated magnetic or polystyrene microbeads, as fibronectin is an ECM-component with an affinity for integrins. Such experiments utilize optical tweezers, magnetic fields, or microneedle probes to apply forces on the order of pico- to nanoNewtons to focal adhesion sites [9, 16, 17].

2.2 Fluid Shear Stress Studies

The effects of fluid flow over cells have been studied, particularly those cells that are subjected to this shear stress physiologically (i.e. endothelial and epithelial cells). Laminar shear stress has been shown to increase the traction force that the cells apply on adherent surfaces, mediated by a shear-induced activation of Rho-GTPase [14]. Altered gene expressions of proteins such as intercellular adhesion molecule-1, vascular cell adhesion molecule-1 (VCAM-1), and E-selectin are also results of shear stress application on vascular endothelial cells [16, 18], as well as changes in the intracellular calcium concentrations [19]. Proposed mechanisms for transcriptional effects have included the transmission of the surface stresses to the nucleus via the cytoskeleton, with a resulting biomechanical activation of gene expression in the nucleus [20, 21], as well as activation of ERK and JNK pathways.

While focal adhesion sites do not appear on the apical surface of cells experiencing fluid shear stress (due to the absence of apical integrin activation by ECM ligands), the role of focal adhesions in the shear stress response cannot be ruled out. The basolateral surfaces of the cells that have been subjected to shear flow studies were replete with focal adhesions, as fibronectin coated the surfaces that the cells adhered to. A force balance on the cell would show that stresses experienced at the apical surface of the cell are matched by the total traction force generated by the numerous interactions between focal adhesions and the fibronectin-coated surface at the basal surface of the cell. Nevertheless, the exact mechanism by which gene expression is affected by shear stress remains a mystery.

2.3 *Finite Element Modeling*

Finite element models (FEM) have been widely used to examine the stress distributions in cells. Although an exact description of the dynamic mechanical properties of the cell is not known, different models have been proposed, each with explanative power of certain experimental observations of cells.

So far, there have been two major categories of cell modeling: the *microstructural* and *continuum* approaches [6]. The first approach considers the cytoskeleton as the primary structural element within the cell, and one famous example of the microstructure approach is the tensegrity model proposed by Ingber [22]. This model posits that cytoskeletal components (microfilaments and microtubules) exist within the cell as an interweaving network that transmits forces and supports itself via interplay between compression and tension.

On the other hand, the continuum model assumes that the cytoplasm is homogeneous, neglecting the microstructure, by considering the length scales characteristic of the dimensions of the cytoskeletal elements. This approach has been used to model the viscoelastic cellular response to the translation and rotation of magnetic beads bound to membrane proteins [5, 23]. Although the continuum approach lends itself to structural modeling, it generally ignores the microstructural elements that comprise the matrix. One of the prevailing mechanical models presented using the continuum approach was proposed by Bausch et al, consisting of a Kelvin body in series with a dashpot [24]. Bausch's viscoelastic model gives rise to a creep response similar to that observed in cells responding to movements of integrin-bound beads. Others have proposed the applicability of the simple Maxwell model to the viscoelastic cell [5], as

forcing of an integrin-bound bead results in an immediate displacement of the bead (unlike what would be seen in a Voigt model). Both Bausch's model and the Maxwell model are presented in Figure 2.2.

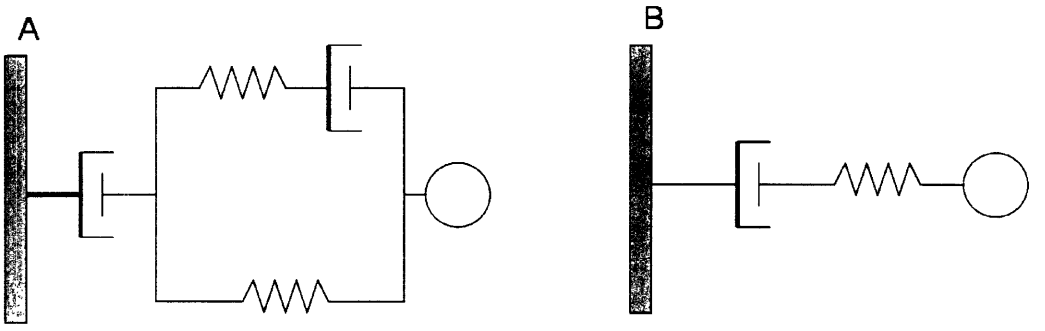

Figure 2.2: Diagrams of two continuum approach models.
A: The model proposed by Bausch et al [24], consisting of a Kelvin body (spring/dashpot in parallel with a spring) in series with a dashpot. B: The Maxwell model, consisting of a spring and dashpot in series.

3.0 MATERIALS AND METHODS

In order to explore the effects of fluid shear stress on focal adhesion activity in an endothelial cell, a two-dimensional, viscoelastic finite element model was developed, and an experiment was designed to verify the model's results.

3.1 Finite Element Model Geometry

Using FEMLAB v. 3.0, a model was created to simulate fluid flow over the surface of a cell, as well as a bead anchored to the surface (see Figure 3). The dimensions of the model estimate the dimensions of a spread endothelial cell, with a length of ~40 μm and a height of ~5 μm. (For two-dimensional models experiencing plane stress, FEMLAB assigns a default width of 0.01. SI units were used in this model,

so the standard width given by FEMLAB was 0.01 m.) The basolateral surface of the cell was attached to a rigid substrate, while the apical surface was exposed to fluid flow. The side surfaces were allowed to move freely. In developing this model, the continuum approach was used, treating the cell as one continuous material (cytoplasm) and ignoring the individual contributions of microfilaments/microtubules network and the membrane / actin cortex layer. The length scale of the microfilament/microtubule network was previously found to be small relative to the length scale of force application by a tethered bead, justifying the continuum approach [5]. Thus, an applied force would have more significant effects in the cytoplasm than in the membrane/cortex layer, as shown by Karcher et al [5]. Furthermore, the nucleus was not considered in the model, even though its material properties differ from those of the cytoplasm. Work by Karcher et al has shown that the stresses due to bead displacement is confined to the region near the bead, and unless the nucleus is found to be very close to the site of the bead, it is unlikely to be affected by bead movement [5].

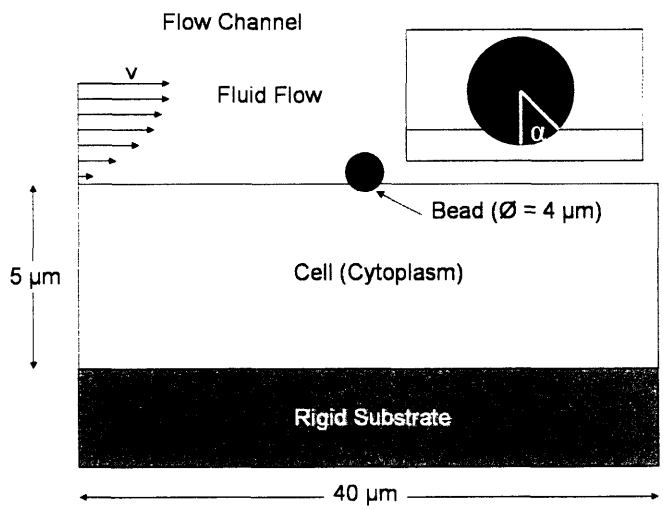

Figure 3.1: Finite element model geometry.
The cell is modeled solely as the cytoplasm. The inset at the top right shows the definition of the contact angle (2α) of the bead with the cell surface. Not to scale.

The bead was given a diameter of 4 μm, as the beads used in subsequent experiments were of this size. Also, beads are coated with an adherent ligand to promote binding to cell surface integrins, and upon binding, form a contact angle (2α) with the surface, as shown in Figure 3. Previous observations have shown that, within an hour after binding, α increases with time, with a mean $\alpha = 67^{\circ}$ [25]. The present model used $\alpha = 60^{\circ}$ to simulate the bead geometry.

The flow channel above the cell was given a height equivalent to the height dimension of the flow channel used in the experiment (400 μm).

3.2 Boundary Conditions

No-slip conditions were applied at the basolateral surface of the cell, at the interface between the cell and the rigid substrate, as well as the fluid-cell and bead-cell interfaces at the apical surface. Free stress conditions were attributed to the side surfaces of the cell. For the flow channel above the cell, a no-slip condition was applied at the top surface. An inlet mean velocity was specified 400 μm before the location of the cell, allowing for flow to fully develop before reaching the cell. The outlet of the channel was given a zero pressure condition.

3.3 Mechanical Properties

Although the exact mechanical properties of the cell are unknown, there has been a general consensus that a viscoelastic model of the cell is valid for a number of experimental situations [24]. Examples of proposed viscoelastic models (Kelvin, Voigt, Maxwell, etc.) are explained above. While none of these models encompass all of the

observed mechanical features of the cell, Karcher et al have shown the reasonable estimation that can result from the Maxwell model, which consists of a spring and dashpot in series [5]. Thus, the Maxwell model was used to characterize the viscoelastic properties of the cell cytoplasm in the present model.

3.4 Material Properties

Previous work has shown that the shear modulus (G) and viscosity (μ) of the cytoskeleton are approximately 100 Pa and 100 Pa·s, respectively [26, 27]. In addition, the Poisson's ratio of the cytoplasm has been calculated to be 0.37 [28]. These values, as well as the density of water ($\rho = 10^3$ kg/m^3), were used for the cytoplasm in the present model.

Both the bead and the rigid substrate were given properties that would characterize them as rigid materials relative to the cell (homogeneous, isotropic, large Young's modulus).

3.5 Fluid Flow Modeling

The fluid flow in the channel over the top surface of the cell was estimated to be laminar, as the Reynolds number,

$$\mathrm{Re} = \frac{\rho v L}{\mu} \tag{1}$$

is in the laminar region (Re~ 50 < 2300) for the characteristic length scale L (μm) of the flow channels used in the experiments. In addition, flow over the cell was modeled in accordance with the Navier-Stokes equation for an incompressible fluid:

$$\rho \frac{\partial \mathbf{v}}{\partial t} + \rho \mathbf{v} \cdot \nabla \mathbf{v} = -\nabla p + \mu \nabla^2 \mathbf{v} + \rho \mathbf{g} \quad (2)$$

The fluid was modeled as water (ρ = 1000 kg/m^3, μ=10^{-3} Pa·s) and was assumed to only contact the cell along the apical surface.

3.6 FEM Solution Techniques

The flow through the channel above the cell and the resulting stress distribution in the cell were modeled in two separate FEMLAB modules: Chemical Engineering and Structural Mechanics, respectively.

The Chemical Engineering module allowed for the modeling of incompressible Navier-Stokes flow within the given rectangular geometry of the flow channel. To determine the inlet velocity of the fluid, the following equation for flow through a rectangular channel was used [29]:

$$Q = \frac{\tau_w \cdot w \cdot h^2}{6\mu}, \quad (3)$$

where the flow rate (Q) is defined as the product of the cross-sectional area of the channel and the fluid velocity. As shear stresses (τ_w) of ~1 Pa have been shown to elicit cellular responses [19, 20], the inlet flow rate needed to generate a shear stress of 1 Pa was calculated to be 0.27 mL/s, corresponding to a fluid velocity of 6.75 x 10^{-2} m/s in the present model. After creating a triangular mesh of the model and solving for the resulting velocity profile, the forces generated upon the apical surface of the cell and bead were outputted from the model.

These forces were then added to the cell-bead surface in the Structural Mechanics module. A triangular mesh of the cell and bead was initialized, with a finer mesh

generated in the region near the cell-bead interface. After solving, the resulting stress distribution throughout the cell and the traction forces imposed on the cell by the rigid substrate were extracted. Additionally, the force values on the cell surface were separated from the force values on the bead; stress distributions and traction forces were calculated for the two isolated forces to determine their relative effects.

3.7 Experimental Design Procedures

In an attempt to design an experiment to verify the accuracy of the FEM results, the following tasks were undertaken.

3.7.1 Bead Coating

To facilitate the binding of beads to cell surface integrins, 4 μm polystyrene beads (Fluospheres F-8858; Molecular Probes, Eugene, OR) were coated with fibronectin, an ECM protein. The coating protocol consisted of washing a 1% 100 μL solution of beads with phosphate buffered saline (PBS) at 4°C and adding fibronectin to give a final fibronectin concentration of 50 μg/mL. The solution was then agitated for 4 hours at room temperature, washed with PBS, and stored at 4°C.

3.7.2 Endothelial Cell Culture and Plating

Bovine aortic endothelial cells (BAEC) were maintained in Dulbecco's modified Eagle's medium (DMEM; Cambrex, East Rutherford, NJ) supplemented with 10% fetal calf serum and 1% penicillin/streptomycin. Cells from passages 6-10 were used.

To enable viewing of focal adhesion sites, the BAEC were transfected with GFP-paxillin vector (from K. Yamada; National Institutes of Health, Bethesda, MD) using FuGene6 (Roche, Indianapolis, IN) with a 3:1 transfection reagent (μL)-to-DNA (μg) ratio.

Since the FEM allowed the cell to move freely at its sides, the cells were plated in the flow channel (Integrated Biodiagnostics μ-Slide 1; München, Germany) such that cells were not in direct contact with each other 24 hours after plating (~100,000 cells in the 5 cm x 5 mm x 0.4 mm channel). One hour before plating, the channel was coated with 100 μl of 150 μg/ml fibronectin and subsequently dried at room temperature. DMEM (600 μL) was added to the wells on each end of the channel after the cell solution was added into the channel.

After the cells had adhered to the bottom surface of the channel and spread (~2-12 hours), 1 μl of the coated bead solution, mixed with DMEM, was added to the channel.

3.7.3 Flow Generation and Fluorescent Microscopy

Approximately 30 min after the addition of the bead solution, a peristaltic pump (Peristaltic Pump P-3; Pharmacia Fine Chemicals AB, Uppsala, Sweden) was connected to the flow channel well using a modified well cap. To achieve steady flow in the channel, a pressurized chamber with one inlet and one outlet port was connected between the pump and the channel.

Before flow was initiated, the channel was placed on the stage of an inverted light microscope (IX-70; Olympus, Melville, NY). Using 60X magnification, a GFP

transfected cell with a bead bound to its surface was located. Once one of these cells was found, flow was initiated at a rate of ~8 mL/min, and images were recorded with a digital camera (CoolSNAP; Roper Scientific MASD, San Diego, CA).

4.0 RESULTS

4.1 Finite Element Model Data

4.1.1 Stress Distribution and Traction Force Solutions

After solving the quasi-static model of incompressible Navier-Stokes flow through a channel, the forces imposed on the apical surface of the cell and on the bead were extracted by an integration of the force over several distinct boundaries. The force values were input into the viscoelastic structural model of the bead-bound cell, and the shear stresses imposed on the cell-bead surface can be found in Figure 4.1. Approaching the bead from the left side of the cell, the shear stress shifts from being predominantly x-directed to having an almost entirely y-directed application; thus the shear stress lifts the left side of the bead. Directly after the bead, the stress values are small (~ 0 Pa in both x- and y-components).

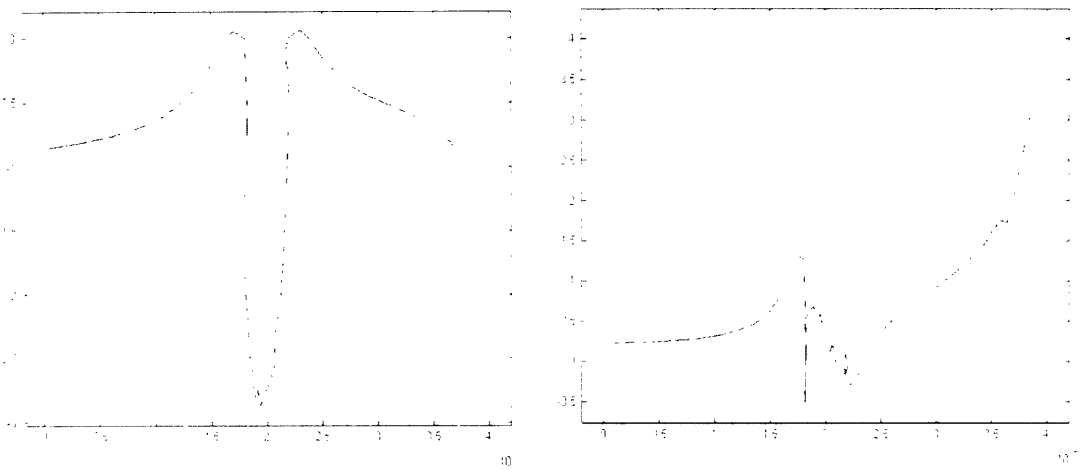

Figure 4.1: Shear stress across apical surface of cell and bead.
Left: x-component. *Right*: y-component. Y-axis values are in Pa.
Note: Negative values signify stress imposed on the bead by the flowing fluid.

The resulting von Mises stress distribution and geometrical deformation of the cell and bead are displayed in Figure 4.2.

The solution to the model was calculated for three different mesh qualities: 318, 1272, and 5088 mesh elements. Calculations with finer meshes could not be achieved with the computer used to create the model (Intel Pentium 4, 3.4 GHz, 1 GB RAM) due to an insufficient amount of memory. Using the results from the two finest meshes (1272 and 5088 elements), bead displacement and maximum stress values differed by 3.38×10^{-5} % and 3.5%, respectively. Thus it is assumed that the 5088 element mesh used in the calculations was adequate to give a solution with <5% error.

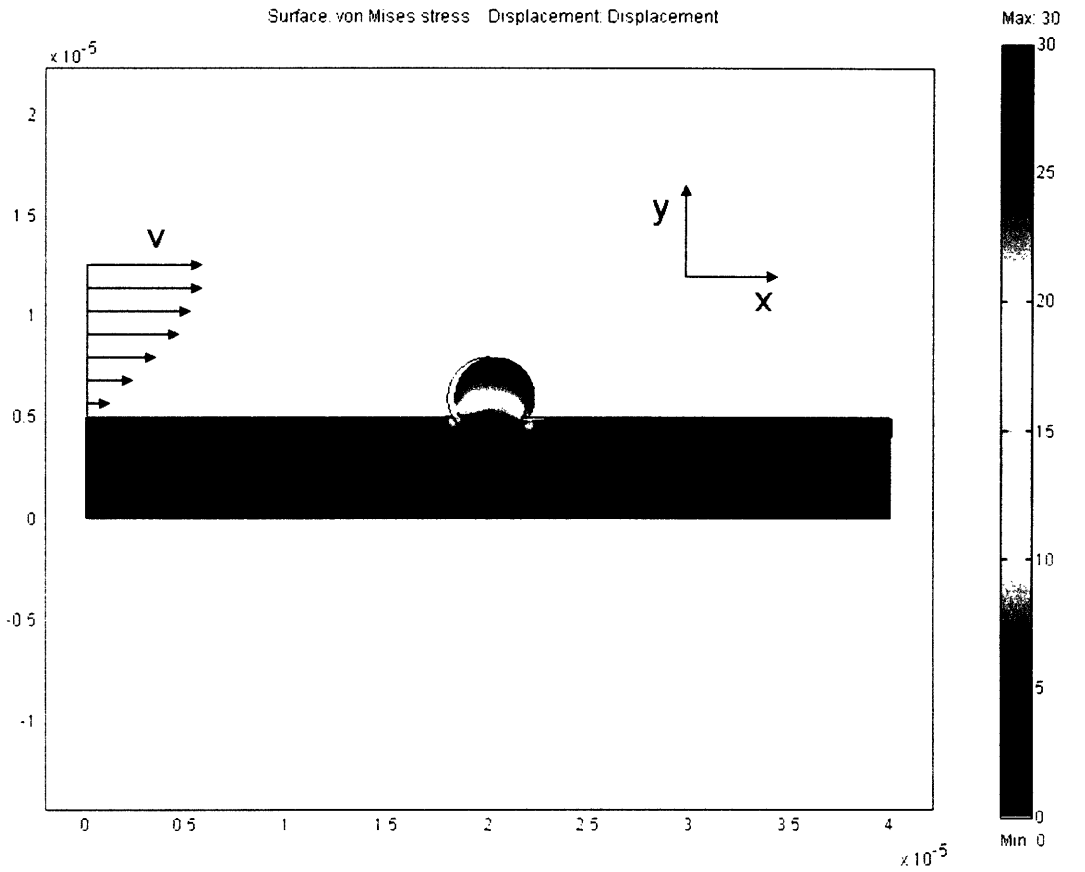

Figure 4.2: Von Mises stress distribution and geometrical deformation of viscoelastic cell model. The velocity gradient of the fluid flow, v, is generated by Poiseuille flow in the channel. This gradient results in a shear stress on the cell and bead, which produces a deformation in the cell-bead geometry. Surface color represents the local von Mises stress, and the color bar gives the corresponding stress values in Pa (ranging from 0 – 30 Pa).

In the model solution, the center of the bead is displaced 3.34 x 10^{-7} m (0.334 μm) in the x-direction, and 1.04 x 10^{-8} m (0.0104 μm) in the y-direction. The bead appears to have rotated clockwise in the direction of flow, as the portion of the apical membrane attached to the left side of the bead shows upward movement, while the portion attached to the right side shows the opposite. The greatest stresses in the vicinity of the bead appear at the leading and trailing edges of the bead-cell interface, and these stresses are propagated approximately half the height of the cell (~2.5 μm) in the vertical direction, and a similar distance in the horizontal direction. However, stresses are still present in almost all regions of the cell, with the exception of the area directly beneath the bead.

Furthermore, large stresses can also be seen be seen at the leading and trailing edges of the cell-substrate interface, likely due to the compressive and tensile forces present in those areas, respectively.

The traction forces that the cell imposes on the substrate at the basal surface were also calculated and are shown in Figure 4.3.

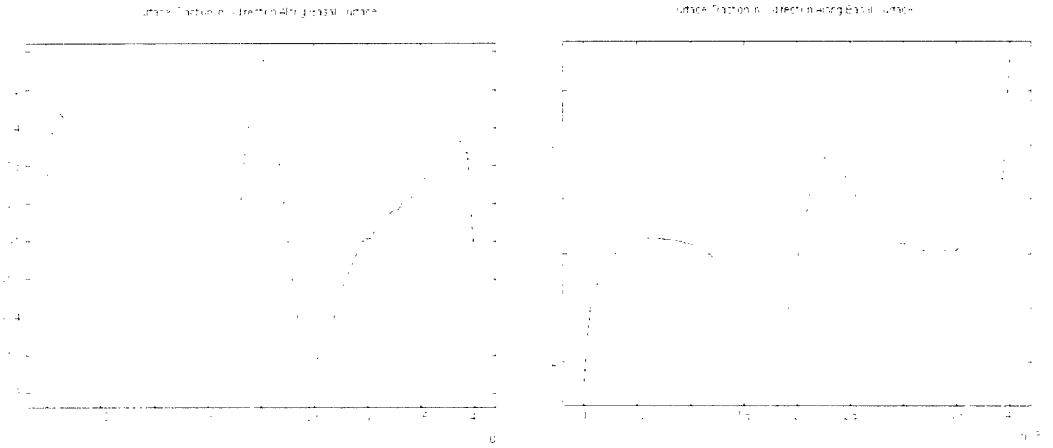

Figure 4.3: Surface traction along basal surface of cell.
The graph depicts the (A) x-component and (B) y-component of the force/area (Pa) imposed on the cell by the rigid binding substrate beneath it. The y-axis is Surface Traction (in Pa), and the x-axis is distance along the length of the cell (in m).

The largest traction forces are found at the bottom right corner of the cell, with a sharp increase in force magnitude that occurs towards the edge of the cell. A similar steep rise in traction force is seen near the left edge of the cell. More force is generated in the vertical direction than in the horizontal direction by an order of magnitude, and the cell pulls up on the substrate in the region before the bead while pushing down on the substrate in the region after the bead. Minimal traction force is seen around the surface directly beneath the bead.

4.1.2 Isolated Contributions

To obtain an estimate of the contributions of the two forces (rotational motion of the bead and the shear stress on the cell surface), solutions were obtained using the force inputs due to only one of the two forces. The stress distribution solutions can be found in Figure 4.4. Not surprisingly, stresses within the vicinity of the bead are shown to be due primarily to the bead's rotation. However, these stresses dissipate fairly rapidly, approaching zero at approximately one bead diameter from the site of maximum stress.

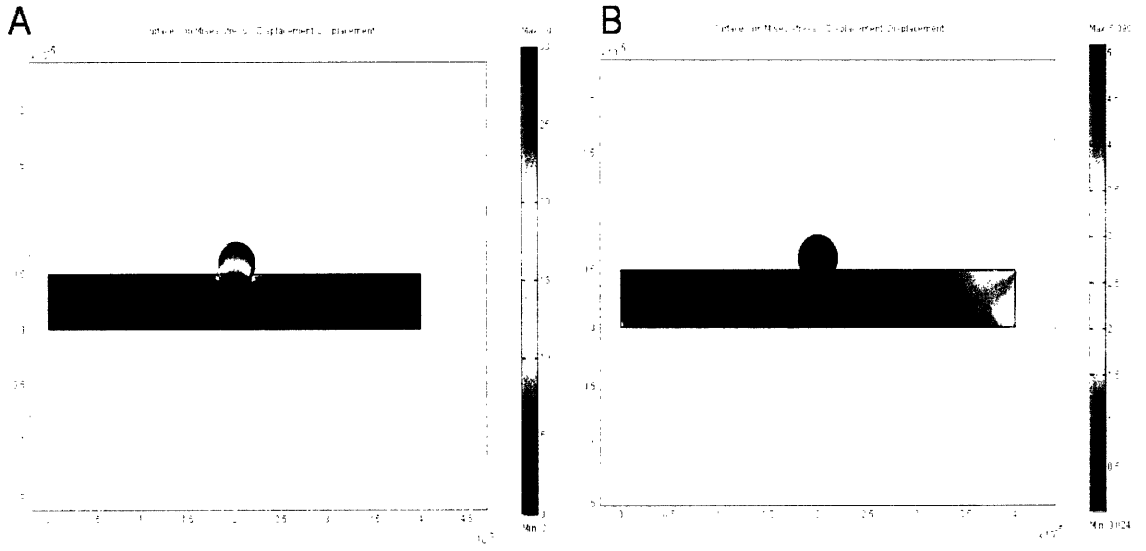

Figure 4.4: Von Mises stress distributions and geometry deformations due to isolated stresses. The stress distribution resulting from: (A) the rotational motion of the bead (stress range: 0-30 Pa), and (B) fluid flow over the cell (stress range: 0-5 Pa) . The geometry deformation is also shown. The color bar expresses the stress values present throughout the model.

Throughout the rest of the cell, the fluid shear stress at the apical surface dominates. Nevertheless, the stresses caused by the fluid shear stress are generally an order of magnitude less than those caused by the bead's rotational motion (~1 Pa vs. ~10 Pa, respectively).

In addition, the traction forces exhibited in each force isolation model were calculated and are shown in Figure 4.3. Compared to the traction forces that result from

the fluid shear stress, the traction forces due to the bead movement are comparable throughout the cell, with the exception of the forces felt towards the edges of the basal surface.

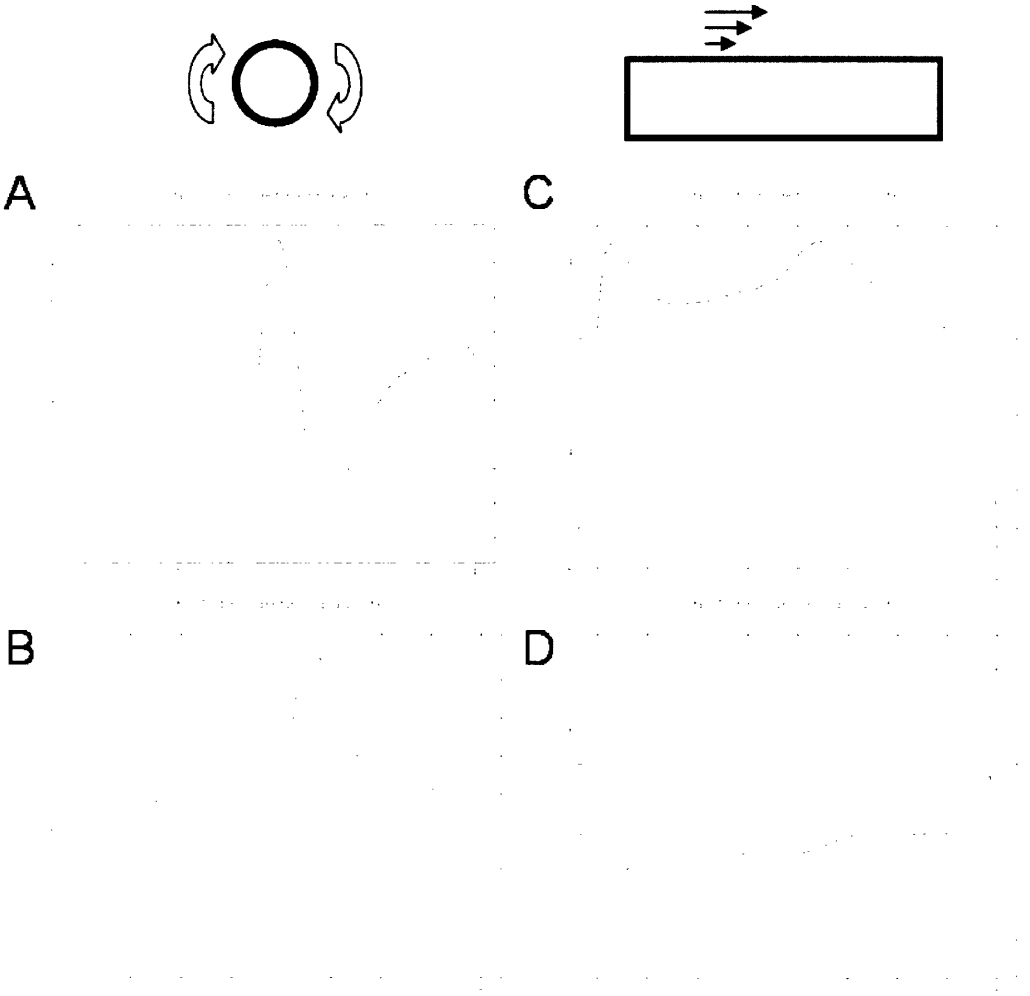

Figure 4.3: Isolated contributions of bead and fluid flow on traction forces at basal surface. The (A) x-component and (B) y-components of the traction force due to the rotational motion of the bead on the apical surface is found in the left half of this figure. The (C) x-component and (D) y-components of the traction force due to the fluid flow over the cell is shown in the right half. The y-axis in all figures is Surface Traction (in Pa), and the x-axis is the distance along the cell (in m).

4.2 Preliminary Experimental Data

As the design of an experiment appropriate for the model setup is still in process, the current experimental data consist only of images. A spread endothelial cell transfected with GFP-paxillin and with two fibronectin-coated beads attached can be seen in Figure 4.4. The fluorescent streaks in the image mark the locations of the numerous focal adhesion sites in the cell. The activity of focal adhesions will thus be analyzed by monitoring the translocations of these streaks in response to fluid shear stresses.

Figure 4.4: Fluorescent image of GFP-transfected endothelial cell with beads attached. Two beads are attached to the cell (solid arrows), and focal adhesion sites (dashed arrows) can be found throughout the cell. Image taken ~48 h after transfection and ~24 h after bead addition.

5.0 DISCUSSION

5.1 FEMLAB Model Contributions

The two-dimensional, Maxwell model of the bead-bound cell under fluid flow provides an estimate of the resulting stress distribution throughout the cell, as well as the forces generated at its basal surface.

5.1.1 Input Stress Values at Apical Surface

Shear stress values at the apical surface of the cell due to flow were calculated using an incompressible Navier-Stokes model in FEMLAB. From this model, the stress along the apical surface to the left and right of the bead were found to be 0.77 and 1.32Pa, respectively. This corresponds to the target shear stress of ~1 Pa.

The stresses along the bead's left and top surfaces were higher (~2-3 Pa), due to the drag force imposed on the cell by the flow. Theoretically, the drag force, F_D, on a sphere (radius a) in a linear velocity gradient of magnitude γ is:

$$F_D = 32\mu\gamma a^2. \tag{4}$$

Although a parabolic velocity distribution is present in the channel, near the bead the velocity gradient can be considered linear due to the relatively small side of the bead and cell (~4-40 μm) compared to the height of the channel (400 μm). This linear gradient has a magnitude of $\gamma \sim 830$, resulting in a theoretical drag force of $F_D \sim 5 \times 10^{-5}$ N. The exposed surface area of the bead in the model is 8.4×10^{-6} m multiplied by the depth of the model (0.01 m). Dividing the drag force by the surface area results in a stress of ~6 Pa. Within the same order of magnitude of the force predicted by the FEMLAB model, the higher theoretical value is likely the result of the fact that only 2/3 of the bead is exposed to the flow and the resulting drag. Therefore, the stress values predicted by FEMLAB are approximately consistent with the expected values.

5.1.2 Stress Distribution

In this continuum model, fluid shear stress was shown to be the primary source of the stresses present in the cell, and the contribution of the bead's rotational motion was

only found in the region near the bead at the apical surface. This localized stress predicted by the FEMLAB model agrees with the results of Karcher et al, whose model showed that the effects of bead movement were confined to distances within approximately two bead diameters [5]. This region corresponds to the site of a focal adhesion, as the bead attaches to the cell via an integrin protein, promoting the formation of a focal adhesion site at the cytoplasmic side of the integrin. Thus, the theoretical model predicts a stress localized to the focal adhesion site.

However, it is difficult to experimentally control the application of stress to a single focal adhesion. Several integrins may be involved in the binding of the bead, considering the bead's larger size relative to integrins. The engagement of several integrins would result in the activation of several focal adhesion sites, and consequently, it would be difficult to attribute any cellular response to a single focal adhesion site.

Furthermore, the continuum model's neglect of the individual contributions of the components of the microfilament / microtubule network is significant. This network directly attaches to the focal adhesion site, providing a structural link between the integrin-bound bead and the rest of the cell. Any stresses on the focal adhesion would be transmitted both locally and globally via cytoskeletal elements. Therefore the stress localization predicted by the continuum is likely not a physiologic reality.

5.1.3 Traction Forces

Calculations for the traction force and stress distribution at the basal surface show that the shear stress imposed by fluid flow is the major contributor to stresses along the basal surface, while the bead's movement results in significant traction forces on the

basal surface regions directly before and after the location of the bead. The model assumes uniform contact of the cell and the substrate at this surface; however in reality, contact is found discretely at focal adhesion sites along the bottom of the cell. Traction forces are thus distributed among the focal adhesions, and the forces deduced from the model give a rough estimate for the forces transmitted to these sites.

5.2 Experimental Design

The current experimental setup, a slight modification of previously conducted experiments, should allow for an analysis of the combined effects of fluid shear stress over the apical surface and the stresses imparted by a subsequently rotating bead. With the use of custom-written MATLAB software (as used by Mack et al and Karcher et al) [5, 9], the positions of the bound bead and the focal adhesion sites throughout the cell can be tracked over time.

While the designed experiment allowed for the observation of beads bound to focal adhesion sites, finding the GFP-transfected cells with beads attached to them was a time-consuming task. The transfection efficiencies achieved in the experiments were rather low (~10-20%), and approximately half of the cells had a bead attached to them at the specified bead concentration. To expedite this location process, a higher concentration of beads could be added into the channel. However, the concentration should not be so high as to facilitate the binding of several beads to a single cell. Since the FEM shows the effects of a single attached bead, additional beads present in the experiment would increase deviation from the model's predictions. Also, attempts to

improve the GFP transfection efficiency would include better mixing of the DNA:FuGene and cell solution immediately after adding the GFP-containing plasmid.

In addition, several parameters can be varied to observe the corresponding cellular responses. For instance, the contact angle of the bead (experimentally varied by changing the amount of time between bead addition and microscope analysis) and the flow rate can be altered to possibly elicit significantly different results.

5.3 Design of a Microfluidic Flow Apparatus

During the course of the experimental design process, a need to study the effects of various media flow rates (and consequently, various shear stresses) was determined. While the flow rate supplied by the peristaltic pump could be varied to achieve different stresses, using this method would require multiple platings of cells to study multiple stresses. A device that would allow for a rapid and efficient analysis of the effects of different shear stresses could be extremely useful for analyzing cellular responses to different levels of mechanical force.

A microfluidic construct was determined to be most amenable to the design needs. Its small length scale requires the use of a minimal amount of resources (media, cells, etc.) and ensures the presence of laminar flow.

5.3.1 Designing for Different Shear Stresses

To determine the dimensions of the channels, a rearrangement of Equation 3,

$$\tau_w = \frac{6\mu Q}{wh^2}, \tag{5}$$

was used to achieve various shear stress values, τ_w. With the peristaltic pumps in the laboratory, the lowest realistic value for Q that can be achieved and maintained is 0.2 ml/min. Also, to help provide a more accurate measurement of the shear stress imposed on a cell, the adherent cell's height should be significantly small compared to the length and height of the channel; amplification of the shear stress value could occur if the cell radius is comparable to the channel length or height [30]. However, for upright microscopes to view the adherent cells at the bottom of the channels, the height dimension must be sufficiently small (~100-200 μm).

Two channels were designed for a media flow rate of $Q = 0.2$ ml/min. Each channel contained two regions of different widths. The first channel had widths of 500 μm and 250 μm, and the second channel had widths of 100 μm and 50 μm. In addition, the height of the channels was set at 200 μm, resulting in shear stress values of 1, 2, 5, and 10 Pa present in the channels. Shear stresses on the order of 10 dynes/cm^2, or 1 Pa, have been required to elicit cellular responses in previous experiments. The shear stresses imposed in the four channels allows for a quick analysis of the effects of various shear stress values (all within one order of magnitude) on cells. The dimensions for the channels and the corresponding shear stress at their bottom surfaces can be found in Table 1.

Table 1: Channel dimensions in microfluidic device design.

Channel	Width (μm)	τ_w (Pa)
1	500	1
1	250	2
2	100	5
2	50	10

Note: Calculated values assume a flow rate of Q = 0.2 ml/min. The length of each channel is ~5 mm, and each channel height is 200 μm.

Determining the length of the channels required an understanding of the length required for fluid flow to fully develop in a channel, a flow characteristic known as the entrance length. A function of the Reynolds number, the entrance length has been shown to be < 1 mm in similar microfluidic (low Re) setups [31]. Therefore, channels ≥ 1 mm were needed to ensure fully developed laminar flow. In the current design, the channels are ~5 mm, so fully developed flow is present in most of the channel. In addition, the channels were given lengths of 5 mm (instead of ~ 1 mm, where flow has fully developed) to increase the number of cells that could be found in each channel. As one major problem in the experiments conducted was finding cells that were both transfected and bound to a bead, the presence of more cells in the channel would increase the likelihood of finding the desired cells. A solid model of the channel design, created with Solidworks 2004 (Solidworks Corp., Concord, MA), can be seen in Figure 5.2.

5.3.2 Designing for Single Cell Analysis

The FEM solves for the effects of fluid shear stress on a single bead-bound cell. To compare the computational results with experimental results, an isolated adherent cell is needed. While plating fewer cells could reduce the confluency of cells in a channel, a more reliable method of plating isolated cells is the "stamping" of fibronectin in certain regions of the channel. Spaced appropriately, these isolated regions of fibronectin coating would promote the adherence of a single cell and facilitate a more accurate comparison of the model to reality.

5.3.3 Fabrication

Fabrication of this microfluidic chip can be carried out using a modified version of the soft lithography method developed by Whitesides et al [32] and a process known as microcontact printing [33]. Microcontact printing allows for the patterning of the local regions of fibronectin on a glass side with the use of a polydimethylsiloxane (PDMS) stamp. First, photopatternable epoxy (such as SU-8) is spin-coated on a silicon wafer. After a photo mask of the desired pattern is produced using computer-aided design (CAD), the photo mask is set flush against the wafer. Placing the masked wafer under an ultraviolet light and subsequently soft-baking it "fixes" certain regions of the wafer by crosslinking the epoxy in the exposed surfaces. A developing reagent is applied to the top of the wafer, dissolving all of the non-fixed epoxy and leaving a negative mold of the PDMS stamp. PDMS is poured over the mold, placed in 70°C temperature for 1 hour, and pulled off of the wafer. The resulting PDMS block contains protrusions corresponding to the desired fibronectin pattern, and these protrusions are dipped into a solution of fibronectin to coat their surfaces. Once coated, the PDMS block is used to stamp the fibronectin onto a glass slide. (See Figure 5.1 for a schematic of the fabrication procedure.). The stamp has 40 μm wide protrusions that span the width of both channels, as endothelial cells spread to approximately 40 μm in diameter after adherence.

Similar methods are used to create a PDMS block with the desired channel pattern etched out. Differences from the procedure mentioned above are the use of a photo mask with the channel pattern printed on and the lack of the fibronectin coating step. Instead, the PDMS block is plasma oxidized and bonded to the fibronectin-patterned glass slide. The result is a microfluidic channel chip with select patches of fibronectin.

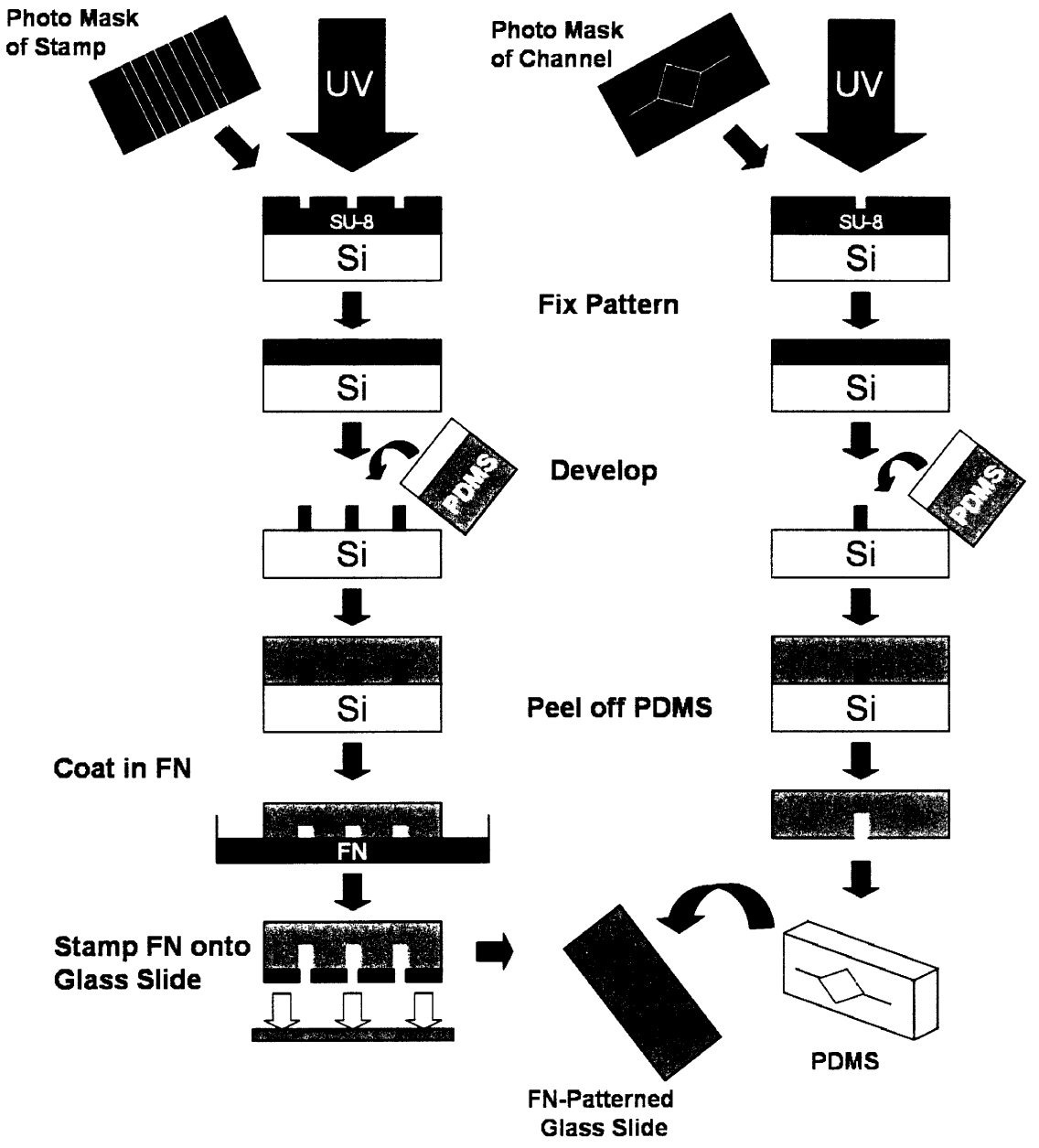

Figure 5.1: Procedure for fabrication of fibronectin (FN) patterned microfluidic channel. See text for a detailed explanation.

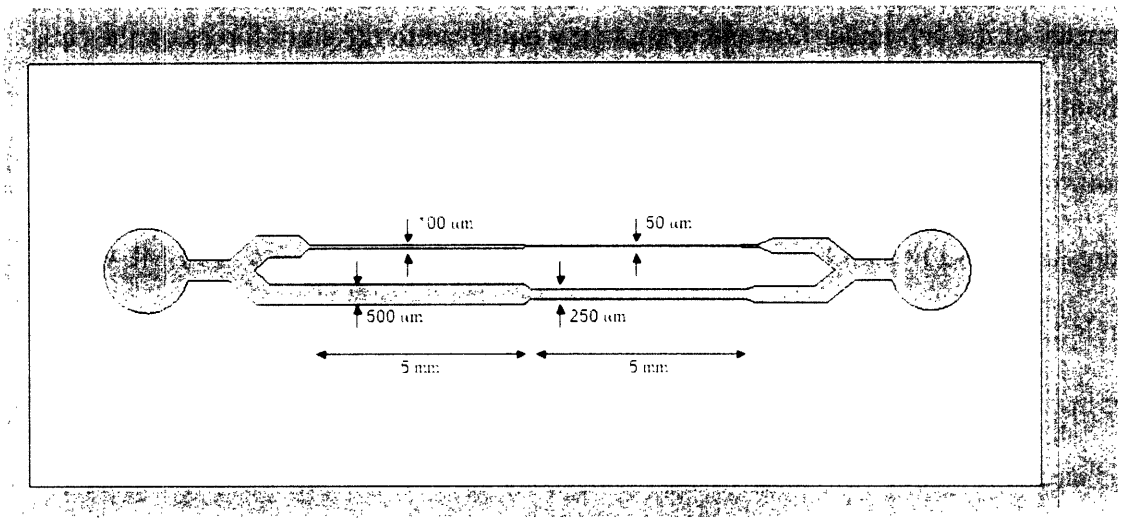

Figure 5.2: Microfluidic channel design.
Flow is directed from the inlet circle at the left to the outlet circle on the right. Channel 1 (bottom channel) exposes adherent cells to shear stresses of 1 and 2 Pa in its 1st and 2nd regions, respectively. Channel 2 (top channel) produces wall shear stresses of 5 and 10 Pa in its 1st and 2nd regions, respectively.

5.4 Recommendations for Future Work

5.4.1 Finite Element Model

Although a two-dimensional model can produce a rough estimate of the stress distribution in a cell, the asymmetric three-dimensional nature of cells require a three-dimensional model to more accurately capture the mechanics of the cell. Also, while no exact mechanical model has been shown to fully encompass all of the cell's features, the Maxwell viscoelastic model contains relatively few cellular characteristics. Thus, a three-dimensional FEM incorporating the more advanced mechanical model proposed by Bausch et al would give more realistic results.

Furthermore, the current model made two significant estimating assumptions. First, the forces applied to the cell by the fluid were not calculated for each point along the geometry. Instead, the stresses along each boundary were integrated over the boundary area, resulting in an estimated force value for 6 boundaries across the top surface of the cell and bead. Secondly, the model did not account for the changing

geometry of the cell under flow, an event that would lead to different forces on the cell. Although assumed to be small due to the small deformation of the cell in the given conditions, a more accurate model would account for the non-static stress application. Addressing these two problems would require the use of a new version of FEMLAB (version 3.2) that will be released in the Fall of 2005. FEMLAB v. 3.2 will enable the coupling of multiple modules, such as the Chemical Engineering and Structural Mechanics modules that were used separately from each other in the current model.

5.4.2 Experimental Methods

After optimizing the methods to produce a higher number of GFP-transfected, bead-bound cells, data on the activity of the focal adhesions on the basal and bead surfaces should be extracted. Work-up of the data could include measurements of focal adhesion translocation under different flow rates and after various bead incubation times (to determine the effect of the contact angle of the bead with the cell membrane). Additional measures to be taken include providing the cells with more ideal experimental conditions. In the current method, media is flown through the channel and over the cells at room temperature, and the cells are observed at room temperature as well. Placing the media source in a 37°C water bath would be one possible solution, but moving the entire experiment apparatus (microscope, flow channel, etc.) into a 37°C warm room or constructing an environmental control chamber for the microscope stage would be most desirable.

6.0 CONCLUSION

Using FEMLAB, a continuum-based FEM of a Maxwell viscoelastic cell was successfully constructed, enabling the analysis of fluid flow over a bead bound to the apical cell surface. The resulting stress distribution was comparable to the results of previous FEMs and was concentrated primarily in the vicinity of the bead, corresponding to the location of a focal adhesion connected to the membrane integrin.

Also, experimental methods and an experimental device were designed to correlate the theoretical FEM results to the observed cellular response. The continued development of the procedures and device, and the subsequent study of focal adhesion movement under flow conditions, will help determine the accuracy of the FEM. Deviations from the model's predictions can shed light on the complex mechanical structure of the cell.

7.0 REFERENCES

1. Davies, P.F., et al., *Hemodynamics and the focal origin of atherosclerosis: a spatial approach to endothelial structure, gene expression, and function.* Ann N Y Acad Sci, 2001. **947**: p. 7-16; discussion 16-7.
2. Wissler, R.W., *An overview of the quantitative influence of several risk factors on progression of atherosclerosis in young people in the United States. Pathobiological Determinants of Atherosclerosis in Youth (PDAY) Research Group.* Am J Med Sci, 1995. **310 Suppl 1**: p. S29-36.
3. Kamm, R.D., A.K. McVittie, and M. Bathe, *On the Role of Continuum Models in Mechanobiology.* ASME International Congress, 2000. **242**: p. 1-9.
4. Tschumperlin, D.J., et al., *Mechanotransduction through growth-factor shedding into the extracellular space.* Nature, 2004. **429**(6987): p. 83-6.
5. Karcher, H., et al., *A three-dimensional viscoelastic model for cell deformation with experimental verification.* Biophys J, 2003. **85**(5): p. 3336-49.
6. McGarry, J.G. and P.J. Prendergast, *A three-dimensional finite element model of an adherent eukaryotic cell.* Eur Cell Mater, 2004. **7**: p. 27-33; discussion 33-4.
7. Haidekker, M.A., N. L'Heureux, and J.A. Frangos, *Fluid shear stress increases membrane fluidity in endothelial cells: a study with DCVJ fluorescence.* Am J Physiol Heart Circ Physiol, 2000. **278**(4): p. H1401-6.

8. Hamill, O.P. and B. Martinac, *Molecular basis of mechanotransduction in living cells.* Physiol Rev, 2001. **81**(2): p. 685-740.
9. Mack, P.J., et al., *Force-induced focal adhesion translocation: effects of force amplitude and frequency.* Am J Physiol Cell Physiol, 2004. **287**(4): p. C954-62.
10. Matthews, B.D., et al., *Mechanical properties of individual focal adhesions probed with a magnetic microneedle.* Biochem Biophys Res Commun, 2004. **313**(3): p. 758-64.
11. Wang, Y., et al., *Visualizing the mechanical activation of Src.* Nature, 2005. **434**(7036): p. 1040-5.
12. Geiger, B. and A. Bershadsky, *Assembly and mechanosensory function of focal contacts.* Curr Opin Cell Biol, 2001. **13**(5): p. 584-92.
13. Geiger, B., et al., *Transmembrane crosstalk between the extracellular matrix--cytoskeleton crosstalk.* Nat Rev Mol Cell Biol, 2001. **2**(11): p. 793-805.
14. Shiu, Y.T., et al., *Rho mediates the shear-enhancement of endothelial cell migration and traction force generation.* Biophys J, 2004. **86**(4): p. 2558-65.
15. Chen, J., et al., *Twisting integrin receptors increases endothelin-1 gene expression in endothelial cells.* Am J Physiol Cell Physiol, 2001. **280**(6): p. C1475-84.
16. Chien, S., S. Li, and Y.J. Shyy, *Effects of mechanical forces on signal transduction and gene expression in endothelial cells.* Hypertension, 1998. **31**(1 Pt 2): p. 162-9.
17. Felsenfeld, D.P., et al., *Selective regulation of integrin--cytoskeleton interactions by the tyrosine kinase Src.* Nat Cell Biol, 1999. **1**(4): p. 200-6.
18. Chiu, J.J., et al., *Shear stress increases ICAM-1 and decreases VCAM-1 and E-selectin expressions induced by tumor necrosis factor-[alpha] in endothelial cells.* Arterioscler Thromb Vasc Biol, 2004. **24**(1): p. 73-9.
19. Shen, J., et al., *Fluid shear stress modulates cytosolic free calcium in vascular endothelial cells.* Am J Physiol, 1992. **262**(2 Pt 1): p. C384-90.
20. Chan, B.P., W.M. Reichert, and G.A. Truskey, *Synergistic effect of shear stress and streptavidin-biotin on the expression of endothelial vasodilator and cytoskeleton genes.* Biotechnol Bioeng, 2004. **88**(6): p. 750-8.
21. Robert, L., *Interaction between cells and elastin, the elastin-receptor.* Connect Tissue Res, 1999. **40**(2): p. 75-82.
22. Ingber, D.E., *Tensegrity: the architectural basis of cellular mechanotransduction.* Annu Rev Physiol, 1997. **59**: p. 575-99.
23. Mijailovich, S.M., et al., *A finite element model of cell deformation during magnetic bead twisting.* J Appl Physiol, 2002. **93**(4): p. 1429-36.
24. Bausch, A.R., et al., *Local measurements of viscoelastic parameters of adherent cell surfaces by magnetic bead microrheometry.* Biophys J, 1998. **75**(4): p. 2038-49.
25. Laurent, V.M., et al., *Assessment of mechanical properties of adherent living cells by bead micromanipulation: comparison of magnetic twisting cytometry vs optical tweezers.* J Biomech Eng, 2002. **124**(4): p. 408-21.
26. Theret, D.P., et al., *The application of a homogeneous half-space model in the analysis of endothelial cell micropipette measurements.* J. Biomech. Eng, 1998. **110**: p. 190-199.

27. Yamada, S., D. Wirtz, and S.C. Kuo, *Mechanics of living cells measured by laser tracking microrheology.* Biophys J, 2000. **78**(4): p. 1736-47.
28. Shin, D. and K. Athanasiou, *Cytoindentation for obtaining cell biomechanical properties.* J Orthop Res, 1999. **17**(6): p. 880-90.
29. Truskey, G.A., F. Yuan, and D.F. Katz, *Transport Phenomena in Biological Systems*. 2004: Pearson Prentice Hall.
30. Walker, G.M., H.C. Zeringue, and D.J. Beebe, *Microenvironment design considerations for cellular scale studies.* Lab Chip, 2004. **4**(2): p. 91-7.
31. Lu, H., et al., *Microfluidic shear devices for quantitative analysis of cell adhesion.* Anal Chem, 2004. **76**(18): p. 5257-64.
32. Sia, S.K. and G.M. Whitesides, *Microfluidic devices fabricated in poly(dimethylsiloxane) for biological studies.* Electrophoresis, 2003. **24**(21): p. 3563-76.
33. Zhang, S., et al., *Biological surface engineering: a simple system for cell pattern formation.* Biomaterials, 1999. **20**(13): p. 1213-20.